



# Optoelectronic properties of highly porous silver oxide thin film

Ahmad Al-Sarraj<sup>1</sup> · Khaled M. Saoud<sup>2</sup> · Abdelaziz Elmel<sup>1</sup> · Said Mansour<sup>3</sup> · Yousef Haik<sup>4</sup>

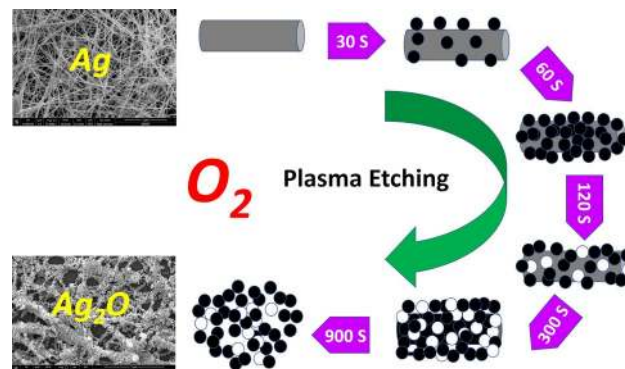
Received: 14 September 2020 / Accepted: 28 December 2020 / Published online: 7 January 2021

© The Author(s) 2021 [OPEN](#)

## Abstract

In this paper, we report oxidation time effect on highly porous silver oxide nanowires thin films fabricated using ultrasonic spray pyrolysis and oxygen plasma etching method. The NW's morphological, electrical, and optical properties were investigated under different plasma etching periods and the number of deposition cycles. The increase of plasma etching and oxidation time increases the surface roughness of the Ag NWs until it fused to form a porous thin film of silver oxide. AgNWs based thin films were characterized using X-ray diffraction, scanning electron microscope, transmission electron microscope, X-ray photoemission spectroscopy, and UV-Vis spectroscopy techniques. The obtained results indicate the formation of mixed mesoporous  $\text{Ag}_2\text{O}$  and AgO NW thin films. The  $\text{Ag}_2\text{O}$  phase of silver oxide appears after 300 s of oxidation under the same conditions, while the optical transparency of the thin film decreases as plasma etching time increases. The sheet resistance of the final film is influenced by the oxidation time and the plasma application periodicity.

## Graphic abstract



**Keywords** Ultrasonic spray pyrolysis · Oxygen plasma etching · Silver oxide film · Optical properties · Electrical properties

**Supplementary Information** The online version contains supplementary material available at (<https://doi.org/10.1007/s42452-020-04091-1>)

✉ Khaled M. Saoud, [s2kmsaou@vcu.edu](mailto:s2kmsaou@vcu.edu); ✉ Yousef Haik, [Yousef.haik@tamuk.edu](mailto:Yousef.haik@tamuk.edu) | <sup>1</sup>College of Science and Engineering, Qatar Foundation, Hamad Bin Khalifa University, Doha, Qatar. <sup>2</sup>Liberal Arts and Science Program, Virginia Commonwealth University in Qatar, Doha, Qatar. <sup>3</sup>Qatar Energy and Environment Research Institute, Qatar Foundation, Hamad Bin Khalifa University, Doha, Qatar. <sup>4</sup>Department of Mechanical and Industrial Engineering, Texas A&M University-Kingsville, Kingsville, TX 78363, USA.

SN Applied Sciences (2021) 3:15 | <https://doi.org/10.1007/s42452-020-04091-1>

## 1 Introduction

The research of new metal oxide nanomaterials thin films deposited on glass substrates has gained much attention in recent years [1, 2] due to their applications in optical engineering [3], sensors [4], biomedicine [5], energy storage [6], and catalysis [7].

Silver (Ag) is known for its valuable properties in many aspects of human life. Properties such as electrical conductivity, antimicrobial, photovoltaic, optical properties, and oxidative catalysis toward many reactions [8–12] make the element superior to other nanostructured metals. Silver has minimal toxicity to humans and has been widely used as a disinfectant and in drug delivery and textile hygiene [13].

Silver oxide systems come in different phases, such as AgO, Ag<sub>2</sub>O, Ag<sub>2</sub>O<sub>3</sub>, and Ag<sub>3</sub>O<sub>4</sub>, creating different types of inorganic materials [12]. Those oxides' crystal structures have different shapes that allow for various optical and electrical properties [14]. As a result, silver oxide has been used as a photocatalyst and in the photovoltaic industry [15] and for energy storage as a cathode in alkaline batteries and many plasmon photonic devices, or as active cathode materials in silver oxide-zinc alkaline batteries [16, 17]. Silver and silver oxide NWs can be used in metal grids to provide high flexibility, high electrical conductivity, and optical transparency [18–20].

Various methods are employed for growing silver oxide thin films, such as thermal oxidation, electron beam evaporation, pulsed laser deposition, chemical vapor deposition (CVD), and DC sputtering [21–26].

The morphology of Ag NWs during and after the synthesis is affected by factors like the reaction temperature, oxidation, and reaction time. Several studies reported the effect of preparation conditions on the length, diameter, and aspect ratio of silver NWs, which result in high transparency, low sheet resistance, and high mechanical properties [19]. Kim et al. reported that a reaction time of 3 h or more could produce Ag NWs with a diameter of approximately 62.5 nm and a length of 13.5 μm [27]. Meanwhile, Atwa et al. reported a high temperature of 170 °C synthesis could yield silver NWs with a length of 15 μm and a diameter larger than 35 nm [28]. Finally, Yang et al. reported an average silver NW with a diameter of approximately 40 nm and an average length of 120 μm, and an aspect ratio of 2500 [29]. Also, the silver oxide nanostructures' morphology and properties depend on the oxidation process and material growth method [30]. Various ways are used to deposition thin films on substrates, such as thermal oxidation, evaporation, CVD, DC sputtering, RF sputtering, and spray pyrolysis [11, 30]. Spray pyrolysis allows for excellent controlling of the thin

film thickness and homogeneity along the substrate. A low-temperature oxidation method based on the cold plasma process is reported by [31]. In this research, we report the influence of oxidation time on the morphology, optical, and electrical properties of silver and silver oxide nonporous NWs. This oxidation process is known for generating nano porosity on the surface of the nanostructure. This porosity affects the electrical and optical properties of the nanomaterial film.

## 2 Experimental

In a typical synthesis, an aqueous solution of silver nanowires (Ag NWs) purchased from Advanced Chemical Supplier Material, LLC, USA) is used in the experiment. The diameter of NWs is 50 nm, while the length is 100–200 μm. The Ag NWs are dispersed in 25 mL of ethanol, and the concentration of the NWs in the solution is 20 mg/mL. The silver NWs solution is diluted in ethanol to better homogeneous deposition and prevent the NWs from clogging the spraying machine's nozzle. An aqueous solution with a 1:20 ratio of silver NWs to ethanol is sprayed on glass substrates made from the highest quality sheet glass. The dimensions of each substrate were 25 × 75 mm, and the thickness was 0.1 mm. The solution is deposited on the substrates using the ultrasonic spraying deposition machine (Exacta coat by Sono-tek). It consists of an impact nozzle, heating plate, and a syringe with a stirrer to pump the solution into the nozzle. The machine deposits the silver on the substrate in the form of tiny droplets (size range in microns) to ultrasonically form piezoelectric crystals.

The crystals control the size of the droplet's mean frequency of oscillation. Pumped gas (nitrogen or argon) then drive the droplets onto the substrate to create a thin film. A computer attached to the machine used to control the coordinates, path, time, and a number of deposition cycles. Pathmaster software is used to program and control the process parameters. The flow rate is controlled by the software and set at 0.8 mL per second, while the air shaping pressure is placed at 0.7 CMM.

A radio-frequency plasma source Plasma etch<sup>®</sup> model PE-100 was used to oxidize the silver NWs. The samples were placed on one of the three horizontally stacked electrodes inside the chamber. The radiofrequency plasma with a power of 30 W is then applied to the silver film under oxygen plasma etching with a mass flow of 15 sccm. The pressure inside the chamber in the vacuum phase was 200 mTor. During the deposition, the temperature inside the chamber is set at 30 degrees Celsius.

The SEM imaging was carried out using FEI Quanta 650 FEG. TEM imaging was done using FEI Talos F200X. Four probe resistance measurements were performed

using the Keithly 2450 source meter. X-ray photoelectron spectroscopy (XPS) was performed using Thermo Scientific ESCALab 250Xi with monochromatic Al K $\alpha$  radiation. X-ray diffraction (XRD) was performed using the Bruker D8 advance, 40 kV, Range 3–90 degrees. Perkin-Elmer 1050 UV–Vis was used for optical measurements. Sheet resistance of the films were measured using the four-point probe technique. In this method, four electrodes are arranged in a linear array. The measurement was performed by injecting a current  $I$  through the sample surface by the two outer electrodes, making a voltage drop  $V$  across the two high impedance inner electrodes that measured using a high impedance voltmeter. Assuming a homogeneous film, the sheet conductance ( $G_0$ ) (siemens (S) unites) is measured by the ratio between voltage to current ratio according to the following equation

$$\frac{I}{V} = \frac{\pi}{\ln 2} G_0 \quad (1)$$

The resistance in ohm ( $\Omega$ ), is calculated by the reciprocal of conductance ( $1/G_0$ ). Since the sheet resistance doesn't change under the scaling of the film contact, it can compare the electrical properties of devices that are different in size [32]. Other researchers widely used this technique to use the four-point probe method to eliminate the instrument lead and contact resistance in measuring the sheet resistance of metal oxide thin films [10].

### 3 Result and discussion

#### 3.1 X-ray diffraction (XRD)

X-ray Diffraction (XRD) was utilized to understand the formation of the silver oxide phase and its crystalline structure during the reactive ultrasonic spray pyrolysis and oxygen plasma etching of the prepared samples. The XRD pattern of the prepared samples of pristine and plasma-treated Ag NWs was highly dependent on the oxidation time, as shown in Fig. 1. X-ray diffraction of the silver oxide films treated in oxygen plasma at different times showed four major broad X-ray diffraction peaks at  $2\theta = 32.3^\circ$ ,  $34.1^\circ$ ,  $37.3^\circ$ , and  $39.6^\circ$  respectively. The strong diffraction peaks at  $2\theta = 32.3^\circ$  and  $37.3^\circ$  related to (111) and (200) Bragg reflections of bulk  $Ag_2O$  (JCPDS 12-0793,  $a = 0.4736$  nm) with a cubic structure [33]. However, the peak at  $2\theta = 34.1^\circ$  is related to monoclinic  $AgO$  (JCPDS 84-1547) [40]. Finally, the peak at  $2\theta = 39.6^\circ$  is associated with the formation of mixed-phase of  $Ag/Ag_2O$ , as reported by [33–35]. No other peaks of other compounds were detected, indicating the high crystallinity and purity of the synthesized sample. These results suggest that the grown silver oxide film is polycrystalline. Upon increasing the oxidation time, the

intensity of  $Ag_2O$  (111) reflection was enhanced, indicating that the crystallinity of the  $Ag_2O$  films was increased. It also suggests a change in the composition of the sample from pristine silver to silver oxide. There was a detection of silver and silver oxide  $AgO$  peaks. The crystallite diameter ( $L$ ) of  $AgO$  nanostructures was calculated using XRD. Full width at half maximum intensity (FWHM) of X-ray diffraction peaks and found to be 13 nm according to the Scherer equation:

$$B(2\theta) = \frac{(k\lambda)}{(L \cos \theta)} \quad (2)$$

where  $B$  is the broadening of the observed diffraction line at its half intensity maximum, and  $k$  is the shape factor, which usually takes a value of about 0.94, and  $\lambda$  is the wavelength of the X-rays used in XRD.

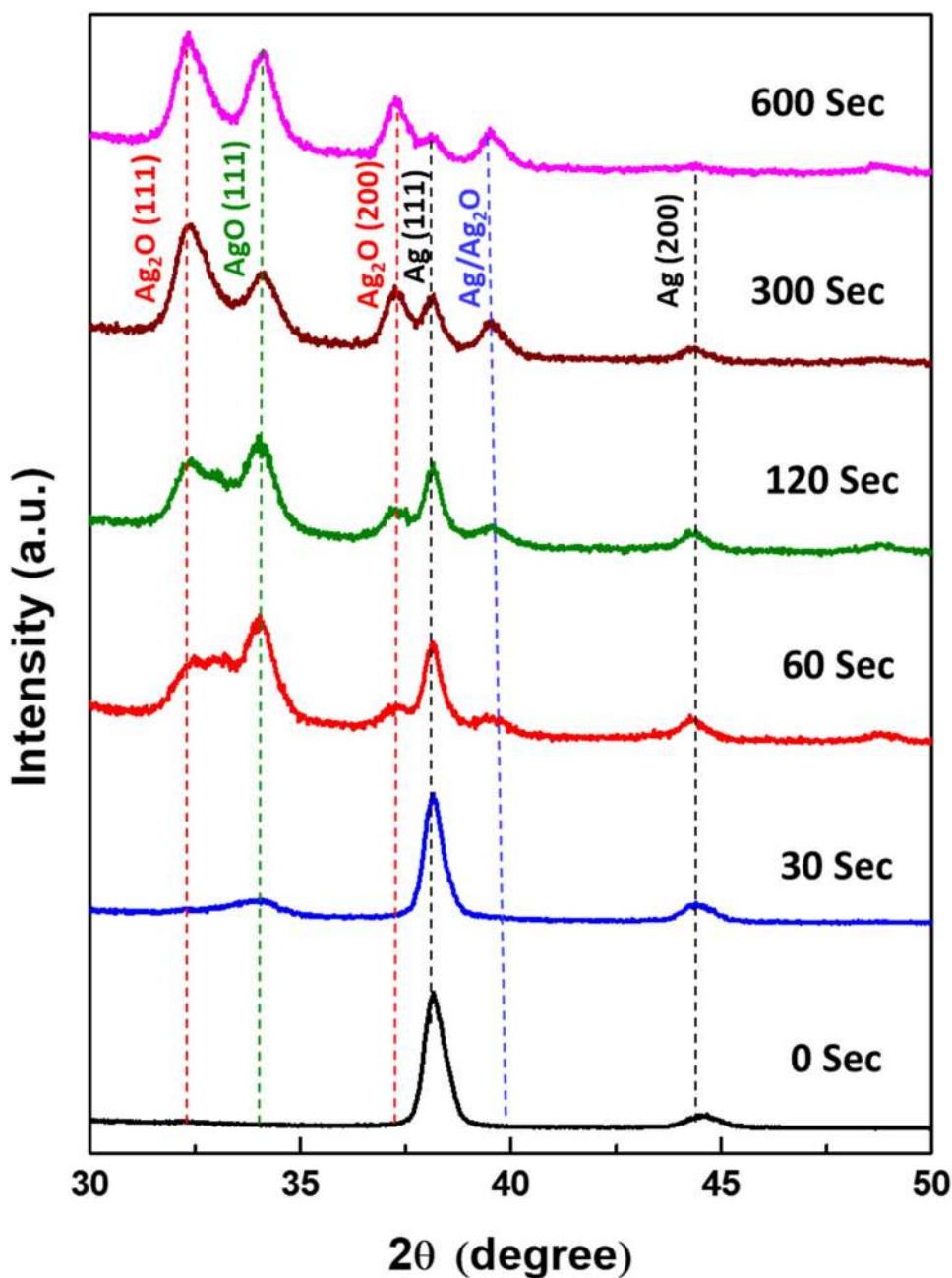
The diffractogram of plasma-treated Ag NWs shows an evolution in the (111) peak intensity of  $Ag_2O$  as we increase the time of exposure to oxygen. The calculated average silver crystalline sizes are 17, 18, 21, 23, and 24 nm for 30, 60, 90, 120, and 300 s. The peak disappears after an oxidation time of 300 s. On the other hand, the calculated average  $AgO$  grain size is between 13 and 17 nm for 120, 300, 600, and 900 s, respectively. The sharp increase in the crystallite at higher oxidation time was due to oxidation of  $Ag$  to  $AgO$  first and then the transformation to  $Ag_2O$  at higher oxidation time.

At zero oxidation time, there is no significant intensity or evidence of the formation of  $AgO$  and  $Ag_2O$  peaks. However, at a greater oxidation time, the rate of formation of  $AgO$  and  $Ag_2O$  oxide becomes more noticeable between 60 and 120 s. The results indicate that as oxidation time increases, the  $AgO$  becomes the dominant oxide. At oxidation time  $> 300$  s, the intensity of  $AgO$  peak decreases, and the peak of  $Ag_2O$  (111) and  $Ag_2O$  (200) increases and, the spectrum agrees well with ICDD card no (00-043-1038) [36]. There was also a formation of a new mixed-phase of  $Ag/Ag_2O$ . Our results agreed well with the results obtained by other researchers [11, 37].

#### 3.2 Film and nanowires morphology

To explore the morphology and size of the generated NWs, we used scanning electron microscopy (SEM) and transmission electron microscopy (TEM). The silver NWs was used in this experiment have a diameter of 100 nm and a length of 100–200  $\mu\text{m}$  sprayed using an ultrasonic pyrolysis machine on glass substrates. RF plasma etching is known and used for silver oxidation and to introduce roughness on the nanowire's surface [31] and hence increase the surface area to volume ratio. The impact of RF plasma exposure time on the morphology and

**Fig. 1** XRD diffraction pattern of Ag NW thin film after RF plasma treatment as a function of oxidation time. For all the conditions, the pressure and the electrical power were 0.23 psi and 30 W, respectively



composition of the nanowire was studied. For this purpose, the oxidation time was varied between 0 and 900 s, while fixing the RF power to 30 W and the oxygen flow to 15 sccm as can be seen in Fig. 2b, after 30 s of oxidation, small lumps of silver oxide form on the surface of the NWs. The mean size of these features is around 20 nm in diameter. The average diameter of NWs increases to 67 nm compared to pure silver NW's shown in Fig. 2a, which have an average width of 100 nm after oxidation, and part of the NWs becomes porous. When increasing the plasma oxidation time to 60 s, the amount of oxide particles covering the Ag NW increases, and the diameter becomes 130 nm

on average, as seen in Fig. 2c. Also, the clusters tend to coalesce together to form more massive clusters along the wires. The Ag NWs become porous after 120 s of plasma etching, and the silver oxide surface clusters almost disappear, and diameter increases to 160 nm, as shown in Fig. 2d. At higher oxidation time (between 300 and 900 s), the NWs become completely porous and sintered in some areas with an average diameter of 300 nm. The aspect (length to width) ratio of the NWs decreases from 2000 in pure silver to 300 in Ag NW's oxidation for 900 s due to the increase of NW's diameter while the length remains almost constant.



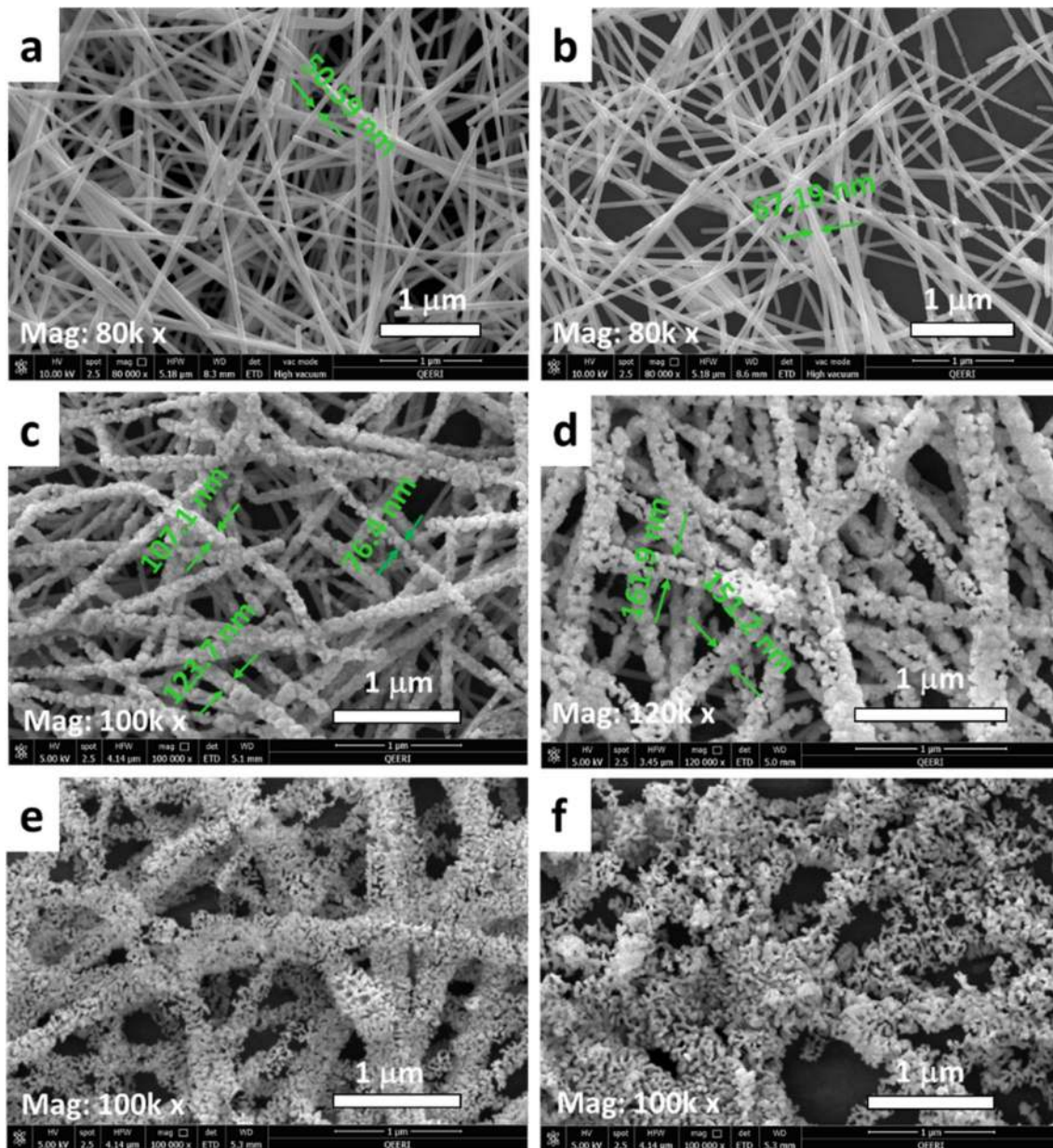


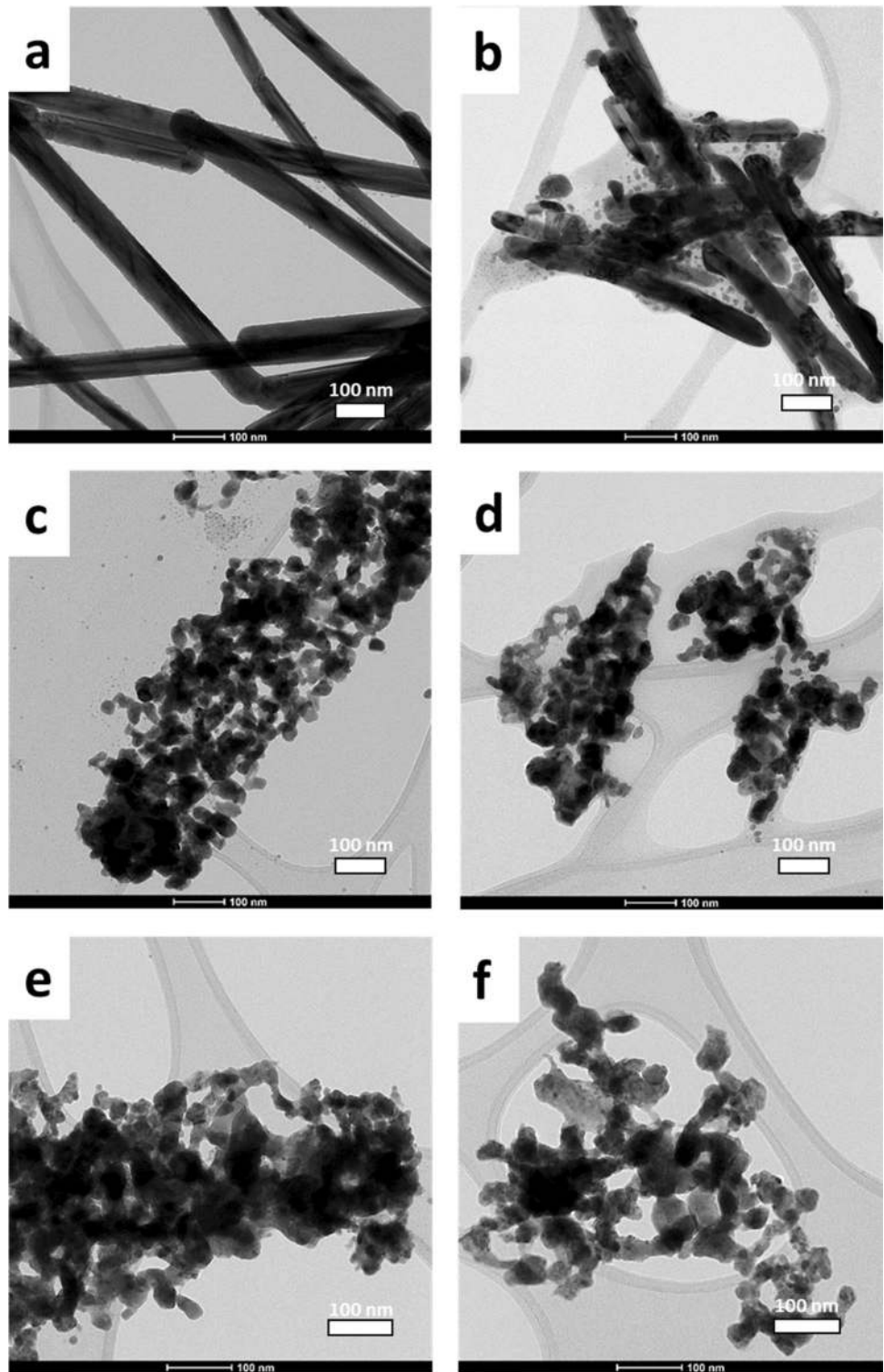
**Fig. 2** SEM micrographs of Ag NW thin film after RF plasma treatment for: **a** 0 s, **b** 30 s, **c** 60 s, **d** 120 s, **e** 300 s, and **f** 900 s. For all the conditions, the pressure and the electrical power were 0.23 psi and 30 W, respectively

TEM was also used to study the morphological and structural changes observed in the different oxide thin film formation stages, as shown in Fig. 3. There is a clear correlation between oxidation time and oxidation of the Ag NWs, as observed by SEM. TEM images for the same samples confirm that nano porosity occurs in the silver NWs after 120 s of oxidation at the chosen etching conditions, as shown in Fig. 3d–g. Moreover, at higher oxidation times from 300 to 900, the wires disintegrate into small pieces distant from each other, which may become

brittle as oxides are brittle and tend to break while Ag-metal is ductile (Fig. 4).

Both SEM and TEM confirm that AgO and Ag<sub>2</sub>O shell covered on Ag NWs, forming the core–shell structure of Ag and Ag oxides, which are explained by the observed increase in Ag diameter. The evolution of oxide formation starts with surface oxidation, and upon increasing the oxidation time, Ag NWs, voids begin to form within the Ag NWS and propagate to the center of Ag nanowire and the loss of internal Ag atoms. Porous AgO/Ag<sub>2</sub>O

**Fig. 3** TEM micrographs of Ag NW thin film after RF plasma treatment for: **a** 0 s, **b** 30 s, **c** 60 s, **d** 120 s, **e** 300 s, and **f** 900 s. For all the conditions, the pressure and the electrical power were 0.23 psi and 30 W, respectively



nanostructures were observed after 120 s of oxidation time. At oxidation time of 300 s, continuous and connected mesoporous AgO and Ag<sub>2</sub>O NWs thin-film finally achieved.

The evolution mechanism of AgO and Ag<sub>2</sub>O NWs thin film formation could be explained as follows: The oxygen

gas particles (O) are active and can oxidize Ag NWs, producing heterostructures Ag and AgO/Ag<sub>2</sub>O forming the Ag/Ag<sub>2</sub>O or Ag/AgO interface. Further oxidation proceeds via Ag<sup>1+</sup> or Ag<sup>2+</sup> rapid out-diffusion by active O particles oxidizing, which lead to the evacuation of central crystallites atoms and the formation of AgO/Ag<sub>2</sub>O as a result of the

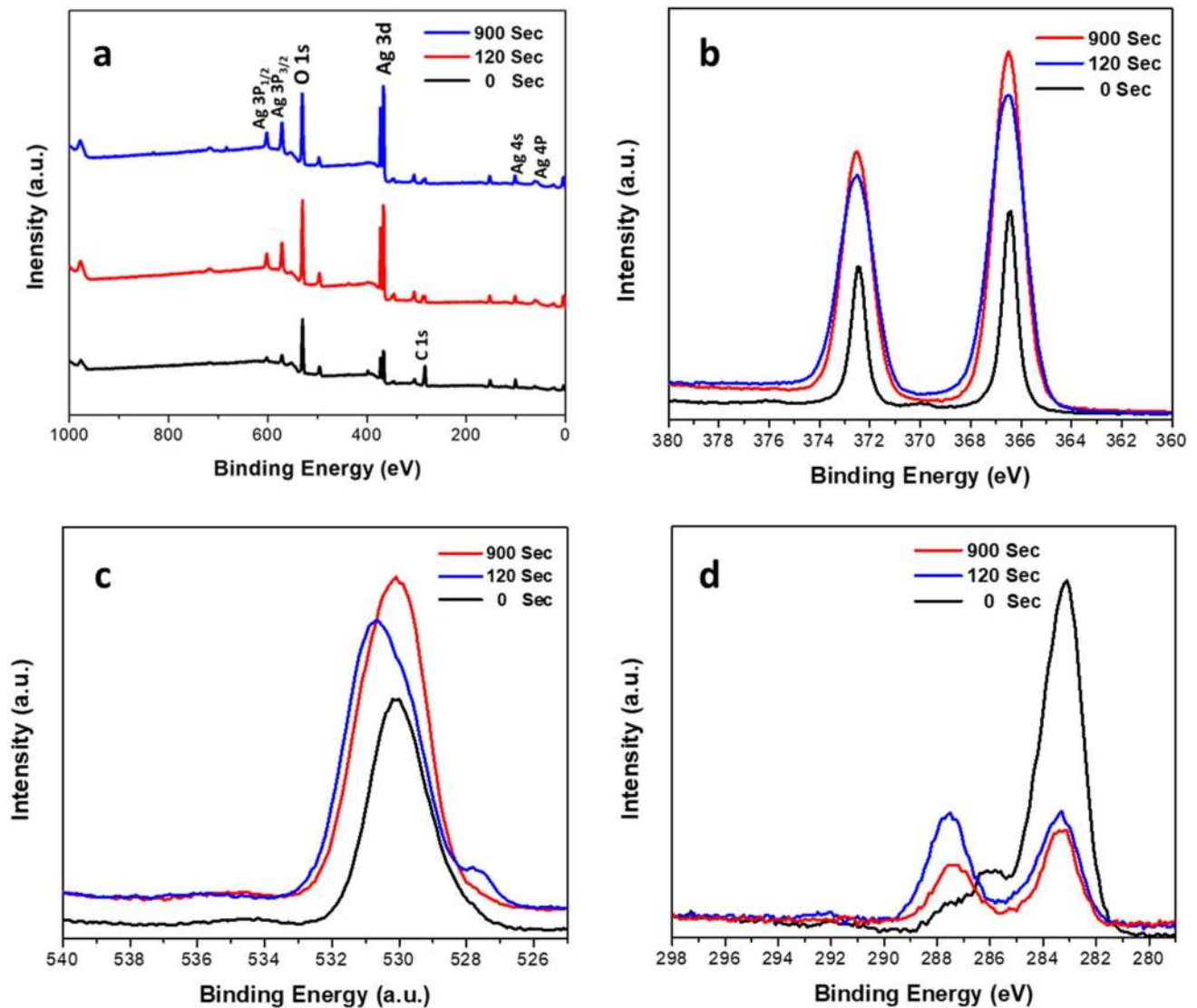
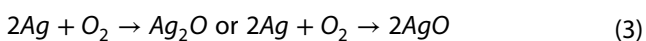


**Fig. 4** X-ray Photoelectron Spectroscopy (XPS) of the Ag NW thin film after RF plasma treatment as a function of oxidation time. For all the conditions, the pressure and the electrical power were 0.23 psi and 30 W, respectively. **a** Survey scan of X-ray photoelectron

spectroscopy (XPS) spectrum of Ag NW thin film. **b** High-resolution Ag3d XPS spectrum of Ag NW thin film. **c** High-resolution O 1s XPS spectrum of Ag NW thin film. **d** High-resolution C 1s XPS spectrum of Ag NW thin film

reaction between Ag NWs and  $O_2$  plasma, which leads to the formation of mesoporous  $AgO/Ag_2O$  nanostructures. Similar results were reported by Li et al. [38]. The transformation of Ag metal nanowires to mesoporous  $AgO/Ag_2O$  process can be explained by the Kirkendall effect where the Oxygen atom is formed in an  $O_2$  plasma mainly via electron impact dissociation to form  $O + O + e^-$  or through dissociative attachment to form  $O + O^-$

The following reactions can express the formation mechanism of  $AgO/Ag_2O$ :



The active atomic Oxygen (O) can easily react with Ag nanowires to form an  $Ag/Ag_2O$  interface, which leads to the formation of an  $Ag@Ag_2O$  heterostructure tube. As the reaction time increased, and due to the rapid out-diffusion of  $Ag^{1+}$  as a result of active atomic Oxygen (O) species oxidation, the evacuation of central crystallites and formation of  $Ag_2O$  shell occurs through the galvanic reaction (Eq. 3) by  $Ag/Ag_2O$  interface between Ag nanowire and  $O_2$  plasma flowed by the formation of mesoporous  $AgO$  and  $Ag_2O$  nanostructure due to the bombardment of the gas molecules. These findings supported by results obtained by several researchers [39–44].



SEM and TEM micrographs of NWS samples oxidized at different oxidation times also indicate that the sample morphology changes from wire-like morphology at low oxidation time to randomly interconnected elongated particles at high oxidation time (after 600 s). The AgO and Ag<sub>2</sub>O particles had a broad grain size distribution of 25–75 nm at 120 s and an average diameter of ~35 nm. After 300 s, the grain size distribution becomes 10–50 nm with an average grain size of ~18 nm. The average silver oxide crystalline sizes calculated from SEM and TEM are slightly higher than the average grain size obtained by X-ray diffraction calculated using the Scherer equation (~22 nm). It is essential to note that the average grain size estimated from the XRD was higher since the XRD signal is from the large particles.

### 3.3 X-ray photoelectron spectroscopy (XPS)

X-ray photoelectron spectroscopy (XPS) analysis to study the modification of surface properties and the oxidation of Ag NWs by ultrasonic spray pyrolysis and oxygen plasma etching method. To better understand the effect of oxidation time on silver and silver oxide NWs, it is crucial to determine the core level binding energies present in the films and the chemical state of both silver and oxygen in the samples. Since XPS can provide beneficial information on the chemical state in the surface of the material, X-ray photoelectron spectroscopy studies performed on the films formed at different oxidation times. The survey scan XPS analysis for the silver and silver oxide NW Film elemental determination formed at different oxidation times shown in Fig. 5a. The XPS survey spectrum of Ag NWs oxidized for 0, 120, 900 min revealed relatively high

phase purity of silver grown oxide films with major elements silver and oxygen (Ag 3d and O 1s), and spectrum of the minor elements such as carbon (C 1s).

In contrast to previously published XPS data for Ag<sub>2</sub>O, which revealed a large number of contaminants by other elements, XPS data shows minor contamination present on our samples' surface. Therefore, these spectra are extremely useful in XPS-studies of Ag-grown oxides [45]. Figure 5b shows the variation of Ag 3d XPS peak intensities of Ag NWs before and after plasma treatment and as a function of oxidation time.

For untreated Ag, the NWs spectrum showed the characteristic core level binding energies at about 366.4 eV and 372.5 eV of the 3d<sub>5/2</sub> and 3d<sub>3/2</sub> peaks spin-orbit splitting of energy levels. The full-width at half maximum (FWHM) for the 3d<sub>5/2</sub> and 3d<sub>3/2</sub> peaks are 0.73 eV and 0.6 eV, respectively. These peaks are in good agreement with previously reported XPS data for Silver oxide [46, 47]. The peaks at 570.9 eV and 601.1 eV, corresponding to Ag 3p<sub>3/2</sub> and Ag 3p<sub>1/2</sub> related to the Ag<sub>2</sub>O films [48]. The O 1s peak at a binding energy of 530.1 eV with full-width at half maximum (FWHM) of 1.9 eV in Fig. (c). shows Ag NW surface oxygen is likely due to atmospheric oxygen and hydrocarbons or oxygen during the synthesis, as reported in the previous reports [47, 49].

Upon exposing the surface of Ag NW to plasma treatment, the contamination on the surface is removed, which is indicated by intensity variation of C 1s peak, at 283.2, and the formation of a new peak at 287.5 as shown in Fig. 5d. The films formed after 120 s oxidation time, the core level binding energy of Ag 3d<sub>5/2</sub> shifted to 366.5 eV, and O 1s shifted to 530.2 eV, and all the peaks were broadened, which could be related to the formation

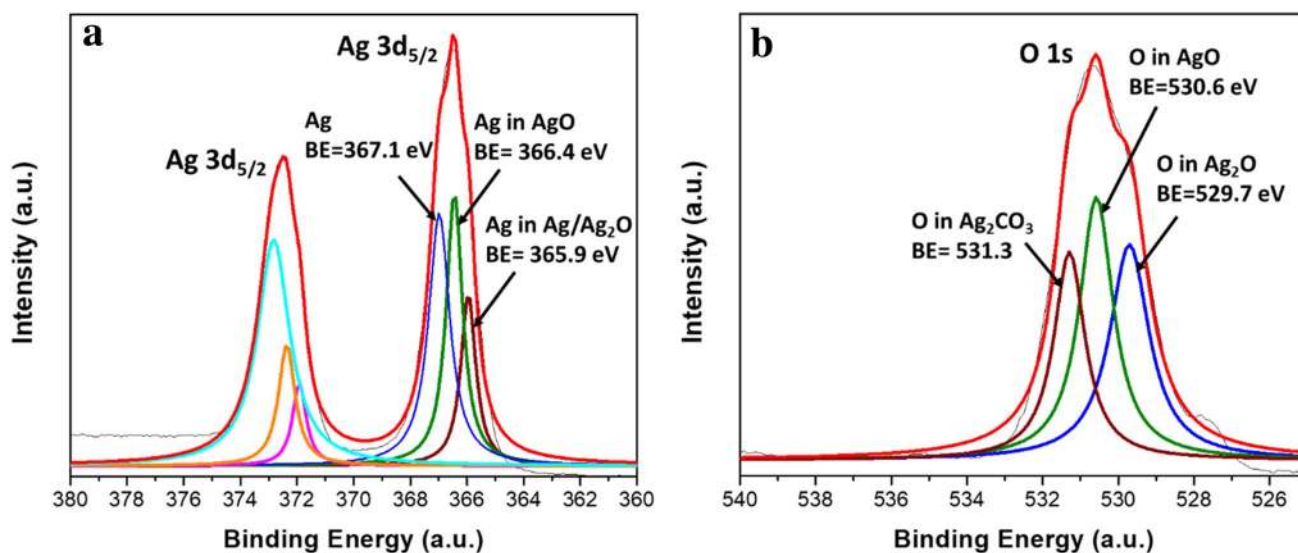


Fig. 5 High-resolution XPS data of **a** Ag 3d<sub>5/2</sub> and **b** O1s peaks of Ag oxide NW thin film after 900 s oxidation time



of AgO and Ag<sub>2</sub>O phases [50]. However, at 900 s oxidation time, the shift becomes higher where the Ag 3d<sub>5/2</sub> shifted to 366.5 eV. In contrast, O 1s shifted to 530.7 eV [51], accompanied by the formation of the new O 1s peak at 527.7 attributed to the formation of mixed-phase of Ag and Ag<sub>2</sub>O and in agreement with observed Ag<sub>x</sub>O phase in the literature [52] as seen in the XRD. These core level binding energies in the films formed at 120 and 900 s oxidation time were in a good agreement with the energies Ag<sub>2</sub>O, as reported by Abe et al. [47, 48] in plasma treated silver nanoparticles. This shift is consistent with previously published reports where the Ag 3d<sub>5/2</sub> core level binding energies in Ag and Ag<sub>2</sub>O and O 1s compared with the pure metallic silver [47, 52].

XPS studies suggest that the films formed at 120 s contained Ag, AgO, and Ag<sub>2</sub>O phases, while those formed at 900 s were of AgO, Ag<sub>2</sub>O mixed-phase, and metallic Ag with Ag<sub>2</sub>O dominant at high oxidation time. Although Ag oxidation state varies in general with a slight difference and due to other factors [51], it is clear that Ag<sup>0</sup>, Ag<sup>+</sup>, Ag<sup>2+</sup> coexisted in the silver oxide film as shown in the fitting the binding energy peak of Ag 3d<sub>5/2</sub> in the high-resolution XPS spectra of Ag<sub>2</sub>O Fig. 5(a). The peaks located at 365.9, 366.4, and 367.1 eV attributed to Ag<sup>0</sup>, Ag<sup>+</sup>, and Ag<sup>2+</sup>, respectively. The peak fitting of O1s in Fig. 5(b) showed O1s XPS spectra of Ag oxide NW thin film, three peaks

at 529.7, 530.6, 531.3 eV attributed to Ag<sub>2</sub>O, AgO, and Ag<sub>2</sub>CO<sub>3</sub>, respectively.

It is important to note that, in the Ag<sub>2</sub>O compound, the Ag 3d<sub>5/2</sub> core level binding energy in the range 367.6–367.8 eV and O 1s were in the range 529.2–529.5 eV, while in pure metallic silver was in 368.0–368.3 eV range [21].

Our results revealed that the films formed after 900 s oxidation time were of mixed-phase of Ag<sub>2</sub>O, AgO, and a mixture of Ag and Ag<sub>2</sub>O, which was also confirmed by X-ray diffraction and X-ray photoelectron spectroscopy studies.

### 3.4 Optical properties

The optical absorption properties of the Ag oxide NW films were investigated by UV–visible spectroscopy to determine the absorption spectrum in the range of 200–800 nm. Figure 3 shows a comparison of the optical absorption spectra recorded for the different silver NW thin film samples at different oxidation times. Absorption is determined by the light that did not pass through the substrate and represented by a percentage after subtracting light transmitted and reflected. All the samples showed a much higher absorption in the visible region due to activation by the visible light [53]. In

**Fig. 6** UV-VIS absorption spectra of Ag NW thin film after RF plasma treatment as a function of oxidation time. For all the conditions, the pressure and the electrical power were 0.23 psi and 30 W, respectively

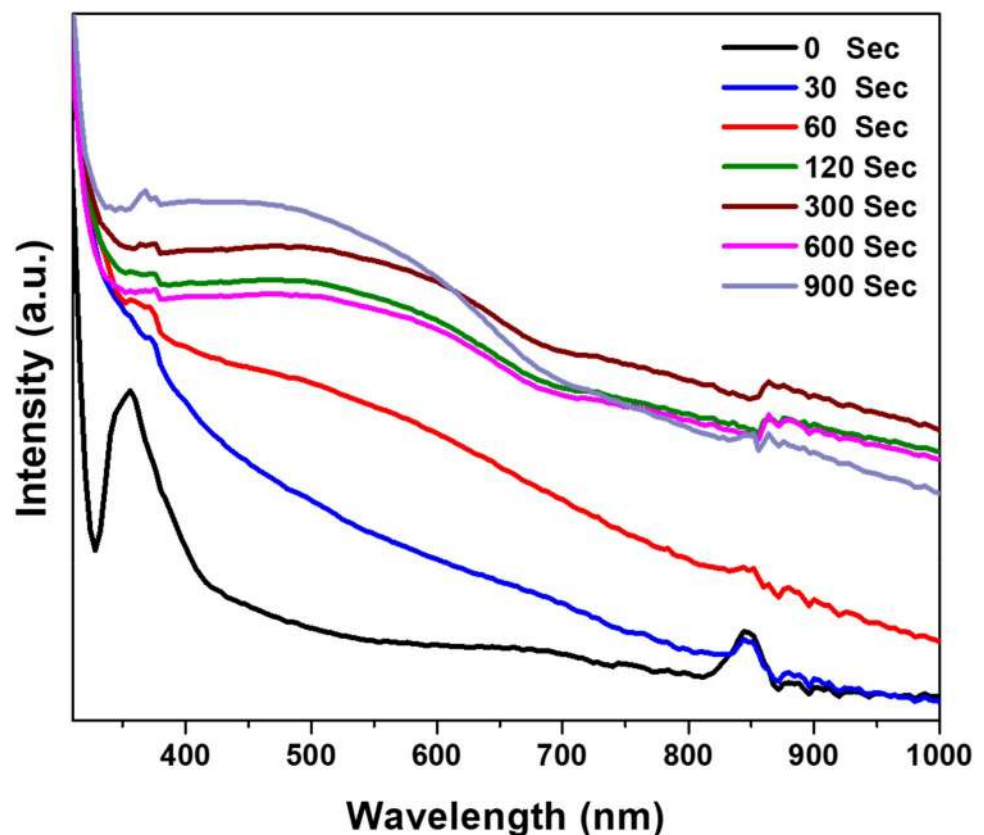


Fig. 6, it is observed that increasing the oxidation time results in an increase in the absorption of visible light and a decrease in transmittance. The Ag oxide NWs have strong absorption in the UV–Visible range with a broad absorption band centered at  $\sim 530$  nm and an absorption tail extending to the NIR region, which indicates that the increment of the oxidation time increases the percentage of silver oxide thickness.

Furthermore, for films made of pristine Ag NWs, the spectra exhibit one peak detected at 357 nm NW [54]. While for samples with oxidation time that varies from 30 s to 900 s, we can notice that absorption increases, and there is no absorption peak. These results can be explained by the increase in the NW's width, as discussed earlier. Also, the percentage of silver oxide in the thin film increases further with oxidation time. Ag NWs showed higher absorption in the blue region of the visible light spectrum which, can be attributed to the photoactivation of silver oxides in this area, which causes the transition from ground to excited states [55]. The absorbance peak of AgNWs in the short wavelength range of 340–380 nm, which shows a strong absorption of near-ultraviolet and short-wavelength visible light around at 356 nm, which is equivalent to a 3.48 eV band gap. However, this peak is red-shifted as the Ag NWs film is transferred to AgO/Ag<sub>2</sub>O to the visible region 450–650 nm, assuming that the film thickness constant. This peak is centered at approximately 550 nm at greater oxidation time, corresponding to a 2.16 eV band gap after 300 s (AgO formation) and 2.25 eV after 900 s oxidation time (after Ag<sub>2</sub>O formation). The optical band gap (E<sub>g</sub>) of starting Ag NW film reported being around 3.48 eV and 2.16 and 2.25 eV for the oxidized Ag NW (AgO) and (Ag<sub>2</sub>O) films. These results suggest that Silver film absorbs less light as the oxidation time increases

and more oxidation results in less absorption. Recent studies report similar results for increasing the oxidation time [56].

UV–Vis spectra are generally used to describe the morphology of nanostructured materials. Silver and silver oxide nanostructures can display surface plasmon resonance (SPR) bands at different frequency ranges [57]. The absorbance peak of Ag NWs occurred in the wavelength range of 340–380 nm and showed strong absorption of near-ultraviolet and short-wavelength visible light, with a significant peak at 369.14 nm and a shoulder at 354.79 nm, both corresponding to typical absorption peaks of Ag NWs [58, 59]. A broad peak was observed between 450–650 nm, which is associated with Ag<sub>2</sub>O metallic nanoparticles [60]. Fakhri et al. studied the effect of annealing Opto-electronic properties of Ag<sub>2</sub>O Films. They found that the incident light wavelength is directly related to the increase in the oxidation temperature and is caused by the transformation of metallic Ag thin films to Ag<sub>2</sub>O [56]. The UV–VIS analysis showed that the optical properties and the film absorption increase as the plasma exposure time increases.

### 3.5 Electrical properties

The electrical parameters of sheet resistance (R<sub>s</sub>) for Ag NW thin films were measured using the four-probe resistance measurement method. The measurement is done by spraying the Ag NW on a glass substrate with four gold electrodes deposited by magnetron sputtering (Fig. 7). Each electrode is connected to a Keithly 2450 source meter with four-probe resistance measurement. The results show that as we increase the plasma oxidation time, the thin film's sheet resistance increases. After 20 s of oxidation, a sharp rise in resistance is observed, and the film becomes

**Fig. 7** Top view of the gold electrode locations and dimensions on the glass substrate for sheet resistance measurements

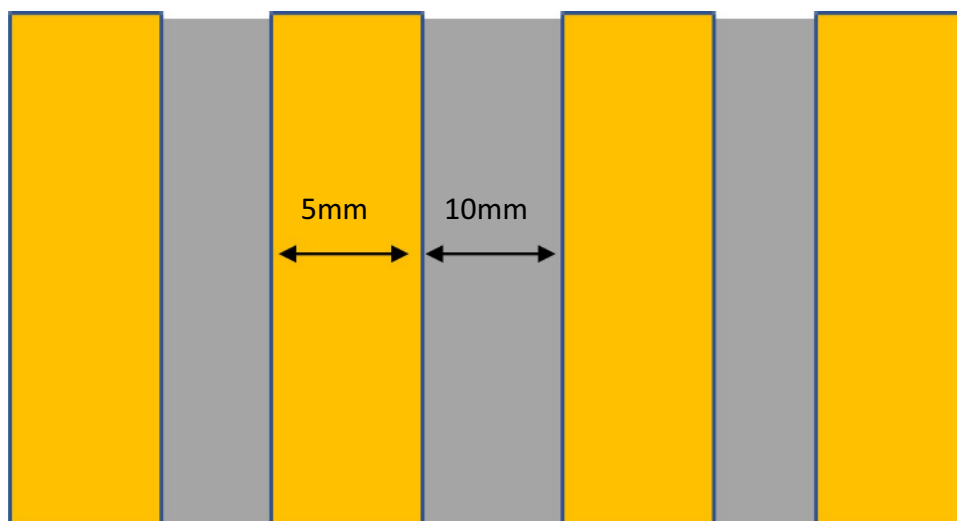
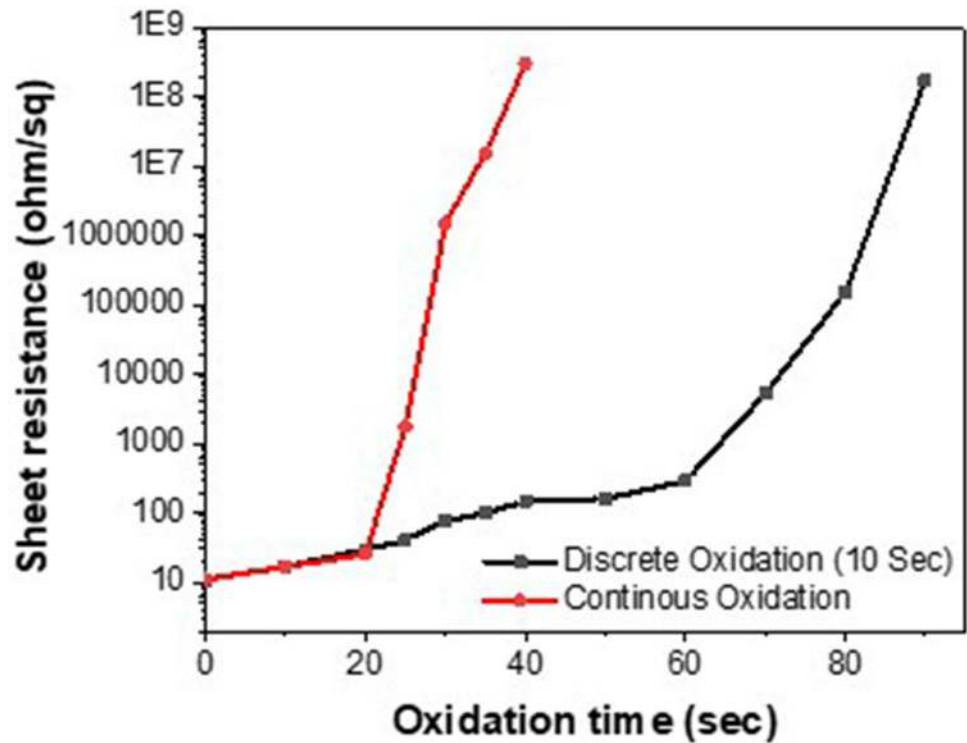


**Fig. 8** Sheet resistance of AgNW thin film after RF plasma treatment. Data in red shows the resistance for samples oxidized for a continuous period. Data in black shows the resistance for samples oxidized for discrete periods of 10 s each



an insulator (Fig. 8), which may be due to the increase of silver oxide amount in the film because silver oxide is a semiconductive material. The increase in porosity and NWs degradation with increased oxidation time reduces the amount of material that can conduct the electrical current along with the film. Also, it might be due to the increase in the grain size of silver, as it was found through XRD analysis that it increases the material's resistance. Applying oxygen plasma for 10 s each result in less sheet resistance compared to an equal period of oxidation in one round. These results could be attributed to the localized heating of NWs acquired through the plasma and accelerated the overall oxidation. In continuous oxidation, the localized heating is no longer there, which delays the transition of silver NWs into silver oxide. Moreover, the nozzle position during spraying pyrolysis plays a crucial role in the resistivity of the film. We found that the closer the nozzle to the substrate, the less resistance of the film with the same number of deposition cycles.

## 4 Conclusion

Porous Ag<sub>2</sub>O NW thin films deposited on a glass substrate have been successfully fabricated by ultrasonic spray pyrolysis and oxygen plasma etching method by exposing the silver NWs to atomic oxygen and transforming them into nanoporous silver oxide NWs upon plasma exposure and oxidation for 120 s. The film morphology, porosity,

electrical, and optical properties are highly influenced by varying oxygen plasma exposure time. XRD and XPS showed that the silver oxide formed at different oxidation times exists in various states of Ag, such as AgO and Ag<sub>2</sub>O or Ag/Ag<sub>2</sub>O mixed phases. The thin film's electrical sheet resistance increases exponentially with an increase in the plasma oxidation time and the plasma exposure periodicity as a result of the formation of an interconnecting thin film.

**Acknowledgements** The authors would like to thank the QEERI Core Labs for valuable SEM, TEM, XPS, XRD, and V-Vis characterization data contribution.

## Compliance with ethical standards

**Conflict of interest** The authors declare that there is no conflict of interest associated with the submitted manuscript and no significant financial support that may have or would have influenced its outcome.

**Open Access** This article is licensed under a Creative Commons Attribution 4.0 International License, which permits use, sharing, adaptation, distribution and reproduction in any medium or format, as long as you give appropriate credit to the original author(s) and the source, provide a link to the Creative Commons licence, and indicate if changes were made. The images or other third party material in this article are included in the article's Creative Commons licence, unless indicated otherwise in a credit line to the material. If material is not included in the article's Creative Commons licence and your intended use is not permitted by statutory regulation or exceeds the permitted use, you will need to obtain permission directly from the copyright



holder. To view a copy of this licence, visit <http://creativecommons.org/licenses/by/4.0/>.

## References

1. Suren S et al (2016) Conductive film by spray pyrolysis of self-reducing copper–silver amine complex solution. *Thin Solid Films* 607:36–42
2. Hameed MS et al (2017) Effect of silver doping on optical properties of nanoflower ZnO thin films prepared by spray pyrolysis technique. *J Mater Sci: Mater Electron* 28(12):8675–8683
3. Nathiya D, Alhaji N, Ayeshamariam A (2019) Inclusion of gallium oxide with silver oxide of tunable optical properties for their unusual catalytic performances. *J Nanosci Nanoeng Appl* 9(2):46–55
4. Lorestani F et al (2015) One-step hydrothermal green synthesis of silver nanoparticle–carbon nanotube reduced-graphene oxide composite and its application as hydrogen peroxide sensor. *Sens Actuators B: Chem* 208:389–398
5. Burduşel A-C et al (2018) Biomedical applications of silver nanoparticles: an up-to-date overview. *Nanomaterials* 8(9):681
6. Mirzaeian M et al (2017) Surface characteristics of silver oxide thin film electrodes for supercapacitor applications. *Colloids Surf A* 519:223–230
7. Trivedi M et al (2015) Silver (I) complexes as efficient source for silver oxide nanoparticles with catalytic activity in A3 coupling reactions. *Inorg Chim Acta* 438:255–263
8. Ma K, An Z (2016) *Macromol. Rapid Commun.* 19/2016. *Macromolecular Rapid Communications*, 37(19): 1632–1632
9. Son WK et al (2004) Preparation of antimicrobial ultrafine cellulose acetate fibers with silver nanoparticles. *Macromol Rapid Commun* 25(18):1632–1637
10. Zhang JH et al (2005) Preparation and absorption properties of polystyrene/Ag/TiO<sub>2</sub> multiple coated colloids. *J Mater Res* 20(4):965–970
11. Saroja G, Vasu V, Nagarani N (2013) Optical Studies of Ag<sub>2</sub>O thin film prepared by electron beam evaporation method. *Open J Metal* 03(04):57–63
12. Tselepis E, Fortin E (1986) Preparation and photovoltaic properties of anodically grown Ag<sub>2</sub>O films. *J Mater Sci* 21(3):985–988
13. Sullivan KT et al (2013) Synthesis and reactivity of nano-Ag<sub>2</sub>O as an oxidizer for energetic systems yielding antimicrobial products. *Combust Flame* 160(2):438–446
14. Hammad A, Abdel-Wahab M, Alshahrie A (2016) Structural and morphological properties of sputtered silver oxide thin films: the effect of thin film thickness. *Dig J Nanomater Bios* 11(4):1245–1252
15. Jiang W et al (2015) Silver oxide as superb and stable photocatalyst under visible and near-infrared light irradiation and its photocatalytic mechanism. *Ind Eng Chem Res* 54(3):832–841
16. Parkhurst WA (1984) Thermogravimetry-evolved gas analysis of silver oxide cathode material. *J Electrochem Soc* 131(8):1739
17. Tominaga J (2003) The application of silver oxide thin films to plasmon photonic devices. *J Phys: Condens Matter* 15(25):R1101–R1122
18. Huang Q, Zhu Y (2018) Gravure printing of water-based silver nanowire ink on plastic substrate for flexible electronics. *Sci Rep* 8(1)
19. Jiu J et al (2014) Facile synthesis of very-long silver nanowires for transparent electrodes. *J Mater Chem A* 2(18):6326–6330
20. Kwon J et al (2018) Recent progress in silver nanowire based flexible/wearable optoelectronics. *J Mater Chem C* 6(28):7445–7461
21. Ekpunobi U (2013) Deposition and characterization of silver oxide from silver solution recovered from industrial wastes. *Am Chem Sci J* 3(3):307–313
22. Ekpunobi U et al (2015) The mechanical properties of ceiling board produced from waste paper. *Br J Appl Sci Technol* 5(2):166–172
23. Mehdi HE, Hantehzadeh MR, Valedbagi S (2012) Physical properties of silver oxide thin film prepared by DC magnetron sputtering: effect of oxygen partial pressure during growth. *J Fusion Energy* 32(1):28–33
24. Gordon R (1997) Chemical vapor deposition of coatings on glass. *J Non-Cryst Solids* 218:81–91
25. Kumar Barik U et al (2003) Electrical and optical properties of reactive DC magnetron sputtered silver oxide thin films: role of oxygen. *Thin Solid Films* 429(1–2):129–134
26. Struppert T et al (2012) Integriertes plasma-monitoring. *J für Oberflächentechnik* 52(9):78–81
27. Kim T et al (2013) Electrostatic spray deposition of highly transparent silver nanowire electrode on flexible substrate. *ACS Appl Mater Interfaces* 5(3):788–794
28. Atwa Y, Maheshwari N, Goldthorpe IA (2015) Silver nanowire coated threads for electrically conductive textiles. *J Mater Chem C* 3(16):3908–3912
29. Li Y et al (2019) One-step synthesis of silver nanowires with ultra-long length and thin diameter to make flexible transparent conductive films. *Materials* 12(3):401
30. Kim M-J et al (2011) Morphological evolution of Ag<sub>2</sub>O microstructures from cubes to octapods and their antibacterial activities. *Bull Korean Chem Soc* 32(10):3793–3795
31. El Mel A-A et al (2016) Creating nanoporosity in silver nanocolumns by direct exposure to radio-frequency air plasma. *Nanoscale* 8(1):141–148
32. Hansen TM et al (2003) Resolution enhancement of scanning four-point-probe measurements on two-dimensional systems. *Rev Sci Instrum* 74(8):3701–3708
33. Waterhouse GIN, Bowmaker GA, Metson JB (2001) The thermal decomposition of silver (I, III) oxide: a combined XRD, FT-IR and Raman spectroscopic study. *Phys Chem Chem Phys* 3(17):3838–3845
34. Pan J et al (2007) Nano silver oxide (AgO) as a super high charge/discharge rate cathode material for rechargeable alkaline batteries. *J Mater Chem* 17(45):4820
35. Zhang R et al (2006) Preparation and characterization of Ag/AgO nanoshells on carboxylated polystyrene latex particles. *J Mater Res* 21(2):349–354
36. Rebelo R et al (2016) Influence of oxygen content on the antibacterial Effect of Ag–O coatings deposited by magnetron sputtering. *Surf Coat Technol* 305:1–10
37. Sajjad S et al (2019) Synergistic evaluation of AgO<sub>2</sub> nanoparticles with ceftriaxone against CTXM and blaSHV genes positive ESBL producing clinical strains of Uro-pathogenic *E. coli*. *IET Nanobiotechnol* 13(4):435–440
38. Li Y et al (2014) Plasma-assisted speedy synthesis of mesoporous Ag<sub>2</sub>O nanotube. *Mater Lett* 126:131–134
39. Chun SR et al (2013) Nanotube arrays: joining copper oxide nanotube arrays driven by the nanoscale kirkendall effect (small 15/2013). *Small* 9(15):2545
40. Donnelly VM et al (2002) Optical plasma emission spectroscopy of etching plasmas used in Si-based semiconductor processing. *Plasma Sources Sci Technol* 11(3A):A26–A30
41. Van Hest MFAM et al (2003) Analysis of the expanding thermal argon–oxygen plasma gas phase. *Plasma Sources Sci Technol* 12(4):539–553
42. Li Y et al (2014) Kirkendall effect induced one-step fabrication of tubular Ag/MnOx nanocomposites for supercapacitor application. *J Phys Chem C* 118(13):6604–6611

43. Niu K-Y et al (2013) Revealing bismuth oxide hollow nanoparticle formation by the Kirkendall effect. *Nano Lett* 13(11):5715–5719
44. Xiaodong H, et al (2016) A 60 GHz four-channel receiver front-end for multiple-beam phased array. In: 2016 IEEE international conference on microwave and millimeter wave technology (ICMMT). IEEE
45. Ferraria AM, Carapeto AP, Botelho do Rego AM (2012) X-ray photoelectron spectroscopy: silver salts revisited. *Vacuum* 86(12): 1988–1991
46. Simon Q et al (2011) Plasma-assisted synthesis of Ag/ZnO nanocomposites: first example of photo-induced H<sub>2</sub> production and sensing. *Int J Hydrog Energy* 36(24):15527–15537
47. Yang Z-H, Ho C-H, Lee S (2015) Plasma-induced formation of flower-like Ag<sub>2</sub>O nanostructures. *Appl Surf Sci* 349:609–614
48. Al Soubaihi RM et al (2018) Silica and carbon decorated silica nanosheet impact on primary human immune cells. *Colloids Surf B* 172:779–789
49. Barreca D et al (2005) Silica-supported silver nanoparticles: tailoring of structure-property relationships. *J Appl Phys* 97(5):054311
50. Wei J et al (2014) Controlled in situ fabrication of Ag<sub>2</sub>O/AgO thin films by a dry chemical route at room temperature for hybrid solar cells. *Dalton Trans* 43(29):11333–11338
51. Weaver JF, Hoflund GB (1994) Surface characterization study of the thermal decomposition of Ag<sub>2</sub>O. *Chem Mater* 6(10):1693–1699
52. Wang X et al (2011) Ag<sub>2</sub>O as a new visible-light photocatalyst: self-stability and high photocatalytic activity. *Chem A Eur J* 17(28):7777–7780
53. Ahmad A, et al (2016) Synthesis of Ag<sub>2</sub>O nano-catalyst in the spherical polyelectrolyte brushes and its application in visible photo driven degradation of dye. *e-Polymers* 16(1)
54. Hu JQ et al (2004) A simple and effective route for the synthesis of crystalline silver nanorods and nanowires. *Adv Func Mater* 14(2):183–189
55. Nwanya A et al (2013) Structural and optical properties of chemical bath deposited silver oxide thin films: role of deposition time. *Adv Mater Sci Eng*
56. Fakhri MA, Bader BA, Khalid FG, Mohammed AZ, Shgathi AA (2016) Annealing effects on opto-electronic properties of Ag<sub>2</sub>O films growth using thermal evaporation techniques. *Int J Nano-electronics Mater* 9:93–102
57. Amendola V, Bakr OM, Stellacci F (2010) A study of the surface plasmon resonance of silver nanoparticles by the discrete dipole approximation method: effect of shape, size, structure, and assembly. *Plasmonics* 5(1):85–97
58. Kuzma A et al (2014) Plasmonic properties of Au–Ag nanoparticles: distinctiveness of metal arrangements by optical study. *J Appl Phys* 115(5):053517
59. Kuzma A et al (2012) Influence of surface oxidation on plasmon resonance in monolayer of gold and silver nanoparticles. *J Appl Phys* 112(10):103531
60. Gallardo OAD et al (2012) Silver oxide particles/silver nanoparticles interconversion: susceptibility of forward/backward reactions to the chemical environment at room temperature. *RSC Adv* 2(7):2923–2929

**Publisher's Note** Springer Nature remains neutral with regard to jurisdictional claims in published maps and institutional affiliations.